Article

Bismuth Vanadate-Nanostructured Graphite Electrodes for Rhodamine B Photoelectrochemical Degradation

Bruna Guimarães Isecke [1], Arthur Saldanha Guimarães [1], Guilhermina Ferreira Teixeira [2], Flavio Colmati [2], Aparecido Ribeiro de Souza [2], Isaac Yves Lopes de Macêdo [1], Lucas Mattos Duarte [3], Sergio Botelho de Oliveira [4], André Gabriel Carmo Costa [1], Vernon Sydwill Somerset [5] and Eric de Souza Gil [1,*]

[1] Faculty of Pharmacy, Federal University of Goiás, Av. Universitária s/n, Goiânia 74605-220, GO, Brazil
[2] Institute of Chemistry, Federal University of Goiás, Av. Universitária s/n, Goiânia 74605-220, GO, Brazil
[3] Institute of Chemistry, Fluminense Federal University, Av. Universitária s/n, Goiânia 74605-220, GO, Brazil
[4] Department of Chemistry, Federal Institute of Goiás, Av. Universitária s/n, Goiânia 74605-220 , GO, Brazil
[5] Department of Chemistry, Cape Peninsula University of Technology, Bellville 7535, South Africa
* Correspondence: ericsgil@gmail.com

Abstract: Electrocatalysis is a promising way to treat water contaminated by harmful organic compounds. The combination of nanoparticles supported on a conductive substrate allows degradation to occur under less energetic conditions. This work evaluated the effect of deposition of bismuth vanadate (BVO) particles on pencil-type graphite electrodes. BVO particles were obtained by ultrasonic irradiation with coprecipitation. Then, they were deposited on the surface of a graphite electrode by the impregnation method. A 2^3-design was used to optimize electrode fabrication. Matter Dispersion Spectroscopy (SEM/EDS), X-Ray Diffraction (XRD) and Dynamic Light Scattering (DLS) were used for characterization. Electrochemical characterization was performed by electrochemical impedance spectroscopy (EIS) and cyclic voltammetry (CV). The results confirmed the synthesis of BVO@C (BVO/graphite). Furthermore, BVO@C significantly increased the electroactive surface area of the electrode, decreased the electron transfer resistance, and significantly increased the electron transfer rate to a greater extent than the electrode without any modification. To prove that the performance of BVO@C is better than the pure electrode, photoelectrocatalysis (PEC) and electrocatalysis (EC) were performed in a rhodamine B (RhB) solution. The results showed that in 5 min of treatment with unmodified electrode, BVO@C EC system and BVO@C PEC system, there was degradation of 31.53%, 46.09% and 58.17% respectively, reaching 95%, 98% and 99.64%, respectively, in 30 min. The reaction rate constants were calculated and to be found k = 0.10272 m^{-1}, k = 0.12221 m^{-1} and k= 0.15022 m^{-1} for the unmodified graphite, BVO@C EC System and BVO@C PEC system, respectively. These results demonstrate that the BVO@C electrodes are efficient for application in a wide range of treatments, including the treatment of organic pollutants.

Keywords: dye degradation; photoelectrocatalysis; organic pollutants; water remediation

1. Introduction

The modification of electrodes with different types of materials, especially semiconductors, has drawn attention in recent years due to their characteristic of being promissory reagents and showing low cost, fast response, portability, increased sensitivity, reduction of overpotentials and resistance to surface fouling. These devices have a wide range of applications, such as in biological research, health monitoring, water and wastewater treatment, clinical diagnosis, and monitoring [1–3].

In environmental treatment processes, advanced oxidative processes (AOP) are successful technologies for treating industrial and sanitary effluents. Among these processes, photoelectrocatalysis with semiconductors is prevalent due to its practical applicability

in a wide range of organic compounds [4]. However, most semiconductor photocatalysts are active in UV light, whose spectral range is present in only 4% of sunlight [5]. To avoid the limitations of UV radiation, many attempts have been made to produce visible photoconductors (VLD). Doping remains a major strategy with semiconductors, sensitizing dyes [6–10], and the heterojunction of different semiconductors [11,12], in which the electrodeposition of metals and their oxides on the semiconductor surface is required [13].

Mixed bismuth oxide systems, e.g., BVO, Bi_2WO_6, Bi_2MoO_6, $BiFeO_3$, $Bi_2Fe_4O_9$, and Bi_5O_7I, have shown high photocatalytic efficiency due to enhanced charge transfer, reducing electron–hole recombination [14–17]. With features such as a narrow band gap (2.3 eV), low toxicity, good dispersibility, and high resistance to corrosion, bismuth vanadate (BVO) has attracted great interest for the degradation of organic pollutants under visible-light illumination. When irradiated at visible wavelength values below 520 nm, BVO exhibits high photocatalytic activity [18].

BVO can present three main polymorphs of scheelite structure: tetragonal zirconia, tetragonal, and monoclinic phase; only the latter shows photocatalytic activity when irradiated under visible light [18]. Due to its semiconductor properties, BVO can also be applied in photoelectrocatalysis (PEC) and electrocatalysis (EC), minimizing the electron hole in the semiconductor material used as a photoelectrode [19].

The photoelectrocatalyst behavior of BVO-based materials can be significantly improved by combining this semiconductor with carbon nanoparticles. This occurs because the carbon nanoparticles store many electrons, making the PEC action of nanocomposites superior to simple semiconductors. In this case, the photogenerated electrons on semiconductors are transferred to carbon nanoparticles, promoting the formation of an abundant number of photogenerated holes accumulated on the semiconductor surface. The photocatalytic properties of m-BVO powder and m-BVO supported on carbon fiber were explored in the degradation of dye. After repeated use in 4 cycles, the photocatalytic action of m-BVO supported on carbon fibers did not show performance loss, while the cycling properties of m-BVO in powder showed poor performance [20].

Based on the theoretical synergy between BVO and carbon [21], the synthesis, optimization, characterization and use of a graphite pencil electrode modified with BVO particles (BVO@C) were evaluated in the present work. For efficiency studies of the obtained electrode, unmodified electrodes and BVO@C were used for Rhodamine B (RhB) degradation.

Semiconductor nanoparticles were obtained by the coprecipitation method and posteriorly deposited on a pencil graphite surface used as the carbon support [22]. This procedure is a low-cost method to obtain photoelectrocatalysts. Improve conditions of m-BVO nanoparticle synthesis were obtained by 2^3 factorial planning. In this study, the electrode obtained from the deposition of BVO on pencil graphite will be referred to as BVO@C.

In addition, electrochemical characterization was performed by Electrochemical Impedance Spectroscopy (EIS) and Cyclic Voltammetry (CV). It has been observed that the formation of nanocomposites from graphite/BVO causes a synergistic effect [21] that aggregates the properties of the two materials. This reduces overvoltage, improves the kinetics of the electrode redox processes, has a progressive effect on mass transfer and increases the sensitivity of the modified electrode, which demonstrates the great potential of using this semiconductor to modify electrodes that can be applied in several studies [22].

For electrode efficiency studies, unmodified electrodes and BVO@C were used for Rhodamine B (RhB) degradation. (RhB) was chosen as it is a cationic dye used for industrial purposes that can irritate the skin, eyes, and respiratory tract when ingested by humans and animals, in addition to being neurotoxic and carcinogenic [23,24].

Due to its harmful characteristics, it is of interest to develop materials capable of preventing this class of compounds in aquatic effluents, thus improving water quality for our consumption. More specific effluent treatment methods aimed at removing persistent compounds are relatively expensive, difficult to apply and time-consuming (reverse osmosis, electrodialysis, adsorption with activated carbon, for example). In addition, recent

works show interest in the application of BVO in photocatalysis and electrophotocatalysis [25–27] since this semiconductor can be activated by visible light instead of UV light, which facilitates the work of degrading emerging contaminants and also allows activation via sunlight [28].

Therefore, the present manuscript aims to develop an electrode based on pencil graphite modified with bismuth vanadate (BVO@C), which is theoretically easy to synthesize and of low cost. This work is also aimed at applying such an electrode to the degradation of different emerging contaminants, which makes this innovative work, as there is nothing similar in the literature regarding pencil graphite electrodes modified with BVO.

2. Materials and Methods

2.1. Materials

Ammonium metavanadate (NH_4VO_3) and basic bismuth subnitrate ($Bi_5O(OH)_9(NO_3)_4$) were purchased from Sigma-Aldrich, Jurubatuba, Brazil, and used without further purification. Nitric acid (HNO_3) (Synth, Brazil) was used to dissolve the bismuth subnitrate. Sodium chloride (NaCl), potassium chloride (KCl), phosphate buffer saline (PBS), potassium ferrocyanide ($C_6FeK_4N_6$), were purchased from Merck S.A. Rhodamine B isothiocyanate (CAS36877-67-7) was purchased from Sigma Aldrich. All solutions were prepared by direct dissolution of the salts in purified water from a Milli-Q plus system (Millipore, Darmstadt, Germany). The graphite used (2b; 2 mm) was purchased from Faber-Castell/Cis (São Carlos, Brazil).

2.2. Preparation of BVO Nanoparticles

BVO powders were prepared by the coprecipitation-ultrasonic irradiation method according to modified procedures previously described [29]: 5.0 mL of NH_4VO_3 (0.43 mol L^{-1}) and 5.0 mL of $Bi_5O(OH)_9(NO_3)_4$ (0.085 mol L^{-1}) aqueous nitric acid solutions (25% v/v) were mixed and sonicated for 1 h at room temperature. For this, a solid steel ultrasonic bath (SSBu-Solidsteel, Piracicaba, Brazil) was used, which uses waves at a frequency of 40 KHz and a volume of 4 L. The yellow precipitate of amorphous BVO formed was separated by centrifuging and washed with distilled water. The final product was dried in the oven at 60 °C and calcinated at 300 °C with an increment of 5 °C/min for 24 h.

2.3. Preparation of BVO@C Electrode

For the preparation of graphite electrodes supported with BVO particles, 2.0 mm 2b graphite (Faber Castell/Cis) was used. Before the deposition of the BVO nanoparticles, the surface of the graphite was prepared in two ways for better adhesion of the particles on graphite. In the first route, all extensions of the graphite surface were evenly sanded with water sandpaper 1200 for 1 min; in the second method, the graphite was immersed in p.a. sulfuric acid. The graphite prepared from both ways was used as the support for BVO particle deposition. In our experiments, we observed that the BVO deposition was better on the sanded graphite surface, so the graphite electrodes applied in the present work were prepared by this route. Graphite sanding was chosen because in preliminary tests it showed better values in relation to BVO deposition compared to pre-treatment with nitric acid. Such results may be correlated with the elimination of the polymeric coating on the pencil surface [30], as well as the removal of impurities present on the graphite surface and the activation of charges on the graphite surface, thus facilitating the adsorption of BVO on its surface. As shown in SEM/EDS, there is the presence of Na, Al, Si, P, K, Ti and Fe in the graphite composition.

Deposits were performed from 30 mL of an aqueous suspension containing different concentrations of BVO nanoparticles (2.5; 5.0; 10.0; 15.0; 20.0, and 25.0 g L^{-1}). Graphite electrodes were kept in contact with the BVO suspension in a shaker at 170 rpm for different times (24, 48, 72, 96, and 120 h). After that, a thermal treatment at 300 °C for 24 h was performed to dry the material.

Factorial Planning

Factorial planning was elaborated to optimize the impregnation of the graphite electrodes with bismuth vanadate film. The planning studied would be the (2^3) + central point, with 2 factors and 3 levels, where the factors were chosen after a preliminary study, being: BVO concentration (15, 20, and 25 g·L^{-1}) and graphite contact time with the vanadate solution (24, 48, 72 h), this being the optimization response of the electrode synthesis obtained through the degradation rate of RhB in 5 min. Table 1 details the conditions of the levels adopted in experiments. Once the variables had been selected, a central compound factorial planning 2^3 + central point (PC) was carried out in triplicate. In this type of planning, the variables are studied in a more significant number of levels, in this way enabling the establishment of an empirical model and the generation of a response surface, which allows the best working conditions to be determined. With this planning data, the ANOVA Table (Analysis of Variance), the response surface, and the contour chart were constructed.

Table 1. Anova table for 2^3 factorial design with center point.

	DF	Sum Sq	Mean Sq	F$_{calc}$	F$_{tab}$ (95%)
R	5	1026.51	205.30	1.27	5.05
r	5	810.90	162,18	0	0
T	10	1837.40	0	0	0
EP	2	146.13	73.06	3.03	19.16
Faj	3	664.77	221.59	0	0

2.4. Materials Characterization

X-ray powder diffraction (XRD) data were collected on a D/max-RB diffractometer (Rigaku, Akishima-shi, Tokyo, Japan) with Cu Kα radiation (λ = 1.54056 Å) at 30 kV, 30 mA, and a 2θ scan rate of 0.3°/min between 15° and 80°. The texture, surface composition, and morphology of the graphite electrode were examined by a Scanning Electronic Microscope (SEM) (SJM—6610, Jeol, Tokyo, Japan) equipped with EDS (Thermo scientific NSS Spectral Imaging, Thermo Fisher Scientific, Waltham, MA, USA). The particle size distribution and zeta-potential of the samples were measured using a Zetasizer Nano ZS analyzer (Malvern Instruments, Malvern, UK) equipped with a He–Ne laser (633 nm, 5 mW). Analyses were performed at NIBS (Non-Invasive Backscatter) and a temperature of 25 °C. The samples were sonicated for 30 min prior to the measurements to assure a homogenous suspension during the measurements. Sonication was necessary to prevent the sedimentation of those particles which were not stable in the used suspensions. Zeta potential was determined by measuring the particle velocity induced under a potential gradient applied across a capillary cell containing BVO powder (Zetasizer, Malvern Instruments Ltd., Malvern, Reino Unido, pH 5.5); the granulometry was measured by dispersing particles in water.

2.5. Electrochemical Characterization

2.5.1. Voltammetric Assays

The voltammetric tests were performed using a PGSTAT$^®$ potentiostat/galvanostat model 204 (Metrohm, Herisau, Suíça) with FRA32M module (Metrohm Autolab, Herisau, Suíçai) ntegrated into NOVA 2.1$^®$ software. To carry out the measurements, an electrochemical cell with a compartment of 25 mL was used, with a system of three electrodes consisting of electrodes (unmodified graphite and BVO@C) and Pt and Ag/AgCl/KCl sat wire (both acquired from Lab solutions, São Paulo, Brazil) representing the work, counter, and reference electrode, respectively.

The experimental conditions for cyclic voltammetry were as follows: sweep rate = 50 mV.s^{-1} and sweep range from −0.4 to 1.0 V. All experiments were performed at room temperature (25 ± 2 °C) in triplicate (n = 3), and the primary electrolyte used was 0.1 mol L^{-1} KCl,

0.1 mol L^{-1} solution (PBS) at pH 7.0. All data were analyzed and treated with Origin 8$^{®}$ software.

2.5.2. EIS Characterization

Electrochemical impedance spectroscopy (EIS) measurements were conducted in a solution containing 0.05 mol L^{-1} potassium ferrocyanide in 0.05 mol L^{-1} KCl over a frequency ranging from 0.1 Hz to 100 kHz at selected potentials for the analysis of the two electrodes, with the application of 0.255 V of potential (DC) and 0.01 V of amplitude (AC) performed at 25 ± 1 °C.

2.6. Photoelectrocatalytic (PEC) and Elecrocatalytic (EC) Systems

To study the photoelectrocatalytic property of the prepared BVO@C electrode, a series of degradation experiments of RhB aqueous solutions under different conditions were performed. The initial concentration of RhB used was 20 mg L^{-1}, with NaCl (0.05 mol L^{-1}) used as the support electrolyte. This concentration was established considering previously performed studies that determined the RhB concentration ranging from 20 to 500 mg·L^{-1} [31]. To carry out the experiment, an energy source was used to which the anode and cathode were connected, and an electric current was applied.

Experiments were carried using a photocatalytic reactor consisting of a wooden compartment composed of six lamps and two coolers, and an electrochemical system composed of two electrodes. The total volume of the solution was 30 mL, and the BVO electrode was used as a working electrode (BVO@C and unmodified electrode), while a platinum wire electrode was used as a counter electrode. The working electrode was irradiated by lamps in the visible range (Osram 220 v and 40 W, Munique, Germany), with a color temperature of 2700 Kλ ≈ 580 nm,) the electric current was kept at 0.02 A, and the voltage kept at 5.0 V. After every 5 min, 2 mL of treatment solution was withdrawn, and changes in RhB absorbance were measured using a UV–Vis spectrophotometer Q798U model (Quimis, Diadema-SP, Brazil) with sweep from 210 to 790 nm.

3. Results and Discussion

3.1. Factorial Planning

In a controlled experiment, considering the variation of the BVO concentration and the contact time of the salt with the sanded graphite, the optimized graphite electrodes supported with BVO particles were obtained. The planning data were submitted for analysis of variance (ANOVA). It was verified, according to the data contained in Table 1, that the model presented a good fit within 95% of the confidence interval. In the case of the ratio between the MQFaj and the MQEP, the F test showed that these two mean squares are statistically equal with an $F_{calc} < F_{tab}$.

The model showed no lack of fit within 95% of the confidence interval (F_{calc} = 3.03 < F_{tab} = 19.16; 2 and 3 degrees of freedom for pure error and lack of fit, respectively). Therefore, a response surface was constructed (Figure 1) to aid the interpretation of the results.

In evaluating the surface, two trends were noticed that seem antagonistic to maximizing the response (more significant degradation of the RhB): (i) longer reaction time (+1) and lower concentration of BVO (−1); (ii) higher concentration of BVO (+1) and shorter reaction time (−1). In both cases, about 85% of RhB degradation was achieved with a reaction time of 15 min. The second case is more interesting to explore due to the relatively low cost that would be added to the prepared photoelectrode BVO@C compared with increasing the contact time of graphite with BVO.

However, the deposition of BVO nanoparticles is not favored by a long contact time between the graphite and the aqueous suspension, since for times longer than 72 h, the graphite begins to dissolve in the reaction medium. In relation to higher values of BVO concentration, it was observed that values greater than 25 g·L^{-1} did not significantly increase the efficiency of RhB degradation. The optimized result for degradation was obtained using the synthesized electrode with 25 g·L^{-1} of BVO and 24 h of contact (experiment 9).
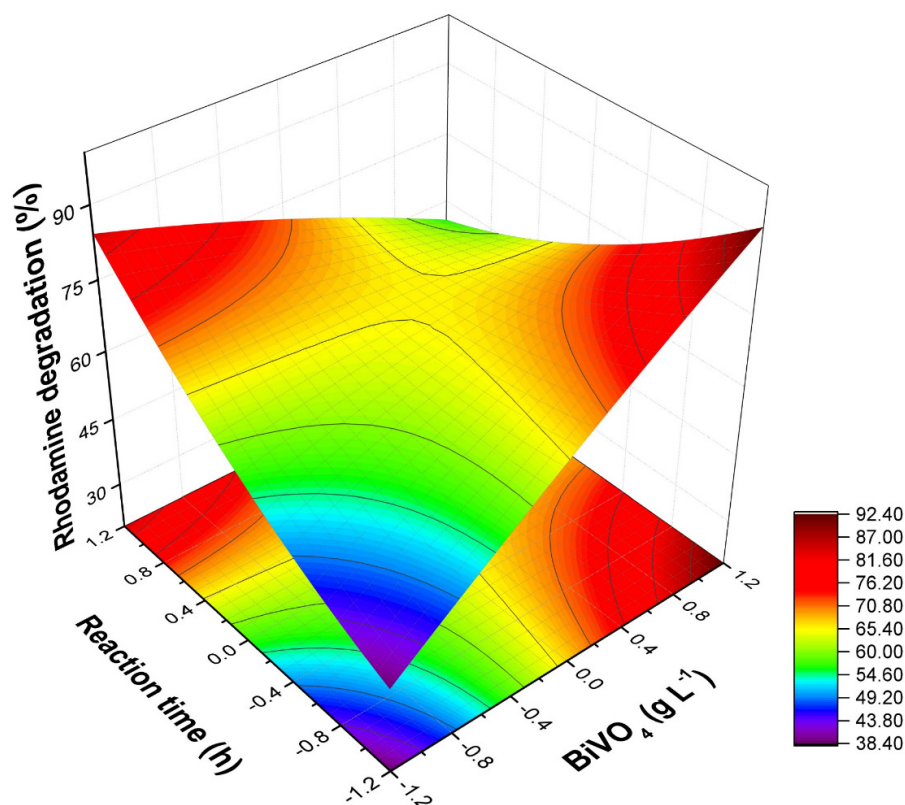
Figure 1. Response surface for the variables' contact reaction time with the semiconductor and BVO concentration.

3.2. Characterization of BVO@C

3.2.1. X-ray Diffraction (XRD)

Figure 2 shows the powder X-ray diffraction (XRD) of pure (BVO) before (BVO1) and after (BVO2) calcination. The samples obtained presented peaks related to the monoclinic scheelite phase of BVO in accordance with JCPDS file no. 83-1699 [32].

The typical XRD patterns of monoclinic BVO [32] present peaks divided into $2\theta = 18.5°$, $35°$, $46°$ and $50°$ [33]; however, for the peak at $18.5°$, this characteristic is better perceived by the insertion referring to the region between $2\theta = 18°$ and $20°$ for all diffractograms represented in Figure 2. Despite the heat treatment, it is observed that there is no perceptible difference between BVO1 and BVO2 in XRD patterns, but the patterns found are quite similar to those described in the literature. A similar result was observed in work related to the fabrication of the FTO electrode doped with a monoclinic film of BVO [34], indicating that heat treatment is an important process for the crystallization of the BVO structure. The monoclinic phase is characterized by more excellent thermodynamic stability and lower band gap value, presenting a crystal structure where the Bi-O polyhedron is more distorted by the $6 s^2$ pair for Bi^{3+} electrons, with an angle of $90.4°$ while in the tetragonal structure, it is more distorted at $90°$ [34].

The extra peaks shown in BVO1 and BVO2 likely correspond to significant amounts of amorphous materials which modify the baseline of diffractograms, making them non-linear and presenting small peaks at the baseline. Sample preparation is considered the biggest source of error for the three fundamental information points of each reflection: angular position, intensity and profile from the peak [33]. In addition, the presence of additional peaks may be related to the preparation of the compound, suggesting that the synthesized material did not present very different peaks from those described in the literature; this may be related to a satisfactory purity and crystallinity for the synthesized BVO1 and BVO2 materials, a result corroborated by other studies [33,34].
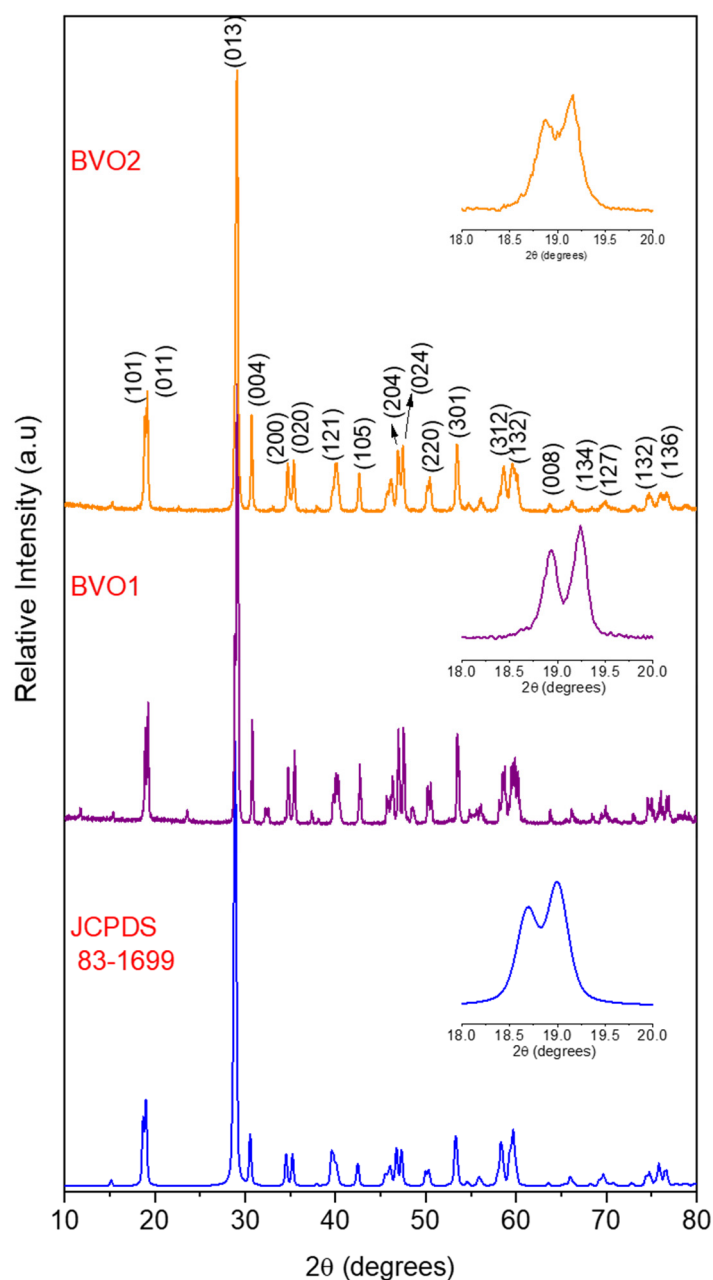
Figure 2. X-ray diffractogram of bismuth vanadate (BVO) before (BVO1) and after (BVO2) thermal treatment at 300 °C for 24 h.

3.2.2. Scanning Electron Microscope and Energy Dispersive Spectroscopy (SEM/EDS)

To investigate the surface characteristics of the modified graphite electrodes, SEM/EDS analyses were performed. SEM micrographs of materials before and after the deposition of BVO nanoparticles, as well as their respective EDS spectra, are shown in Figures 3 and 4. As can be seen in Figure 3a,b, the sanding step in the preparation of the electrode allows the deposition of BVO. Peaks referring to Na, Al, Si, P, K, Ti and Fe were found in the XRD analysis; this might be explained by the fact that the graphite pencil currently consists of a mixture of graphite and clay or mortar (mainly SiO_2) whose ratio varies with the grade of pencil (4B, 2B, 5H and etc.). In this way, peaks referring to compounds present in the clay and mortar that make up pencil lead are also shown in Figure 2. Some studies carried out show that clays and mortars have Al_2O_3, Fe_2O_3, TiO_2, K_2O, MgO, ZnO, SiO_2 and other compounds in their composition [35–37].

Figure 3. SEM images of pencil graphite surface: (**a**,**b**) before the deposition of BVO particles; (**c**) EDS spectrum indicating the composition of material after deposition.
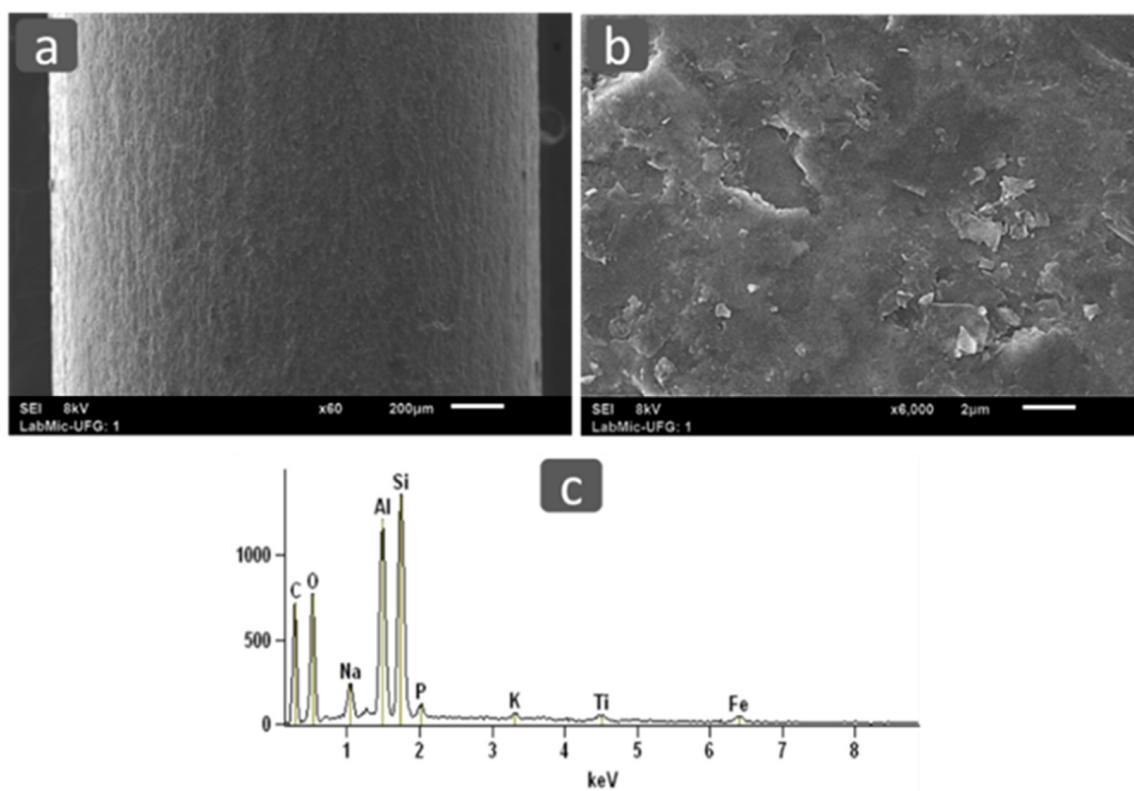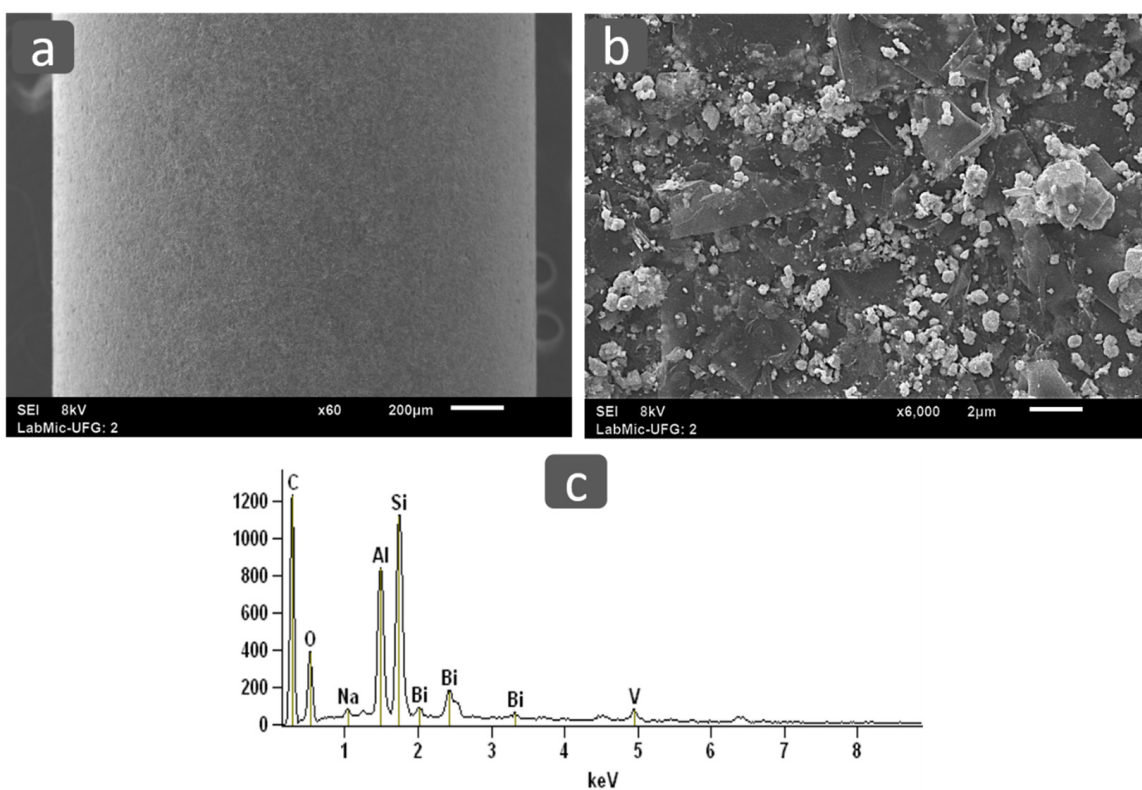

Figure 4. SEM images of pencil graphite surface: (**a**,**b**) after the deposition of BVO particles; (**c**) EDS spectrum indicating the composition of material after deposition.

The surface of the graphite electrode presents some irregularities, and some particles are observed on the surface of graphite after the deposition process (Figure 4b); in addition, it is noticed that the particles present different size. These results are supported by EDS after deposition, with the spectrum shows peaks referring to Bi, V, and O (Figure 4c).

As the temperature used for the heat treatment of the electrodes was the same used in the synthesis route, and the particles used in the deposition process were previously prepared and characterized by X-ray diffraction (Figure 2), it is possible to assume that the particles on the surface of graphite consist of monoclinic BVO. As observed in Figure 4b, the graphite surface was not homogeneously covered by BVO particles, which may be related to the Polydispersity Index (PDI) values found. Furthermore, after deposition, the EDS spectrum also shows peaks related to carbon electrons (Figure 4c).

3.2.3. DLS and Zeta Potential Measurements

Some photocatalytic semiconductors have altered behavior in the aqueous medium [38]. To further investigate the properties of BVO, the hydrodynamic particle size was analyzed, and about 98.5% (peak 1) of the powder showed values of approximately 0.3328 μm while about 1.5% (peak 2) of the powder showed a diameter of 5.56 μm and with a mean value of 0.4184 d.μm. The polydispersity index (PDI) was 0.456, which represents an intermediate value of monodispersity for the solution. It is not known what constitutes an acceptable number for the PDI, but values close to 0.2 indicate that the solution is more monodispersed, that is, without the probable formation of "clusters" of the analyzed compound. It merely has to be suitable for the purpose. The presence of peak 2 with much larger diameter values of BVO powder is not interesting because to have better coverage of the substrate, it is necessary that the molecules have lower values. As for the realization of the electrode synthesis experiments, the BVO was subjected to a long time in shaker; this factor could have been reduced. The values found from the DLS were compatible with those determined by SEM (0.017–0.886 μm).

This result is essential since a more significant dispersibility over a greater surface area guarantees a more excellent surface available for electrocatalytic and photoelectrocatalytic reactions. However, these PDI values can also be correlated to the non-formation of a BVO film on the graphite surface, as seen in the SEM analysis, since the water/BVO solution is very monodispersed. The zeta potential found on the surface of the BVO@C material was $\zeta = -22.2$ mV, indicating that the surface charge of the particles used to modify the graphite presented negative charges. Theoretically, semiconductors with negative surface charges will be more efficient in degrading cationic organic pollutants. In addition to Rhodamine B, other cationic dyes include acridine orange, proflavine, safranin, neutral red [39], methylene blue [40], malachite green [41], and crystal violet. Some pharmaceutical compounds (e.g., ciprofloxacin and norfloxacin, amitriptyline, clozapine, verapamil, risperidone, and hydroxyzine [42]) are also cationic, along with several other persistent organic pollutants.

3.3. Electrochemical Characterization

Electrochemical Impedance Spectroscopy (EIS) was used for the characterization of interfacial variations of the electrode surface, and also to investigate impedance behaviors based on different electrodes. In EIS, the rightmost part of the semicircle in the Nyquist plot corresponds to the resistance associated with electron charge transference, i.e., the electrode's resistance to charge transference (Rct), followed by an c.a. 45° ascendant line, which is related to the diffusion process in the electrode. Moreover, the diameter of the semicircle represents the difficulty of electron transfer in the solution and electrode system, providing information on the resistivity of the system and on the electrochemical interphase.

Figure 5 shows Nyquist diagrams for EIS measurements for the unmodified electrode and for the BVO@C. Through the analysis of the diagrams, a small-diameter semicircle was observed for the unmodified electrode, the diameter of which was smaller in BVO@C (0.01 kΩ). These results suggest that the surface of BVO@C modified with BVO particles has a lower resistivity to electron transference between the electrode/solution interface.

The improvements observed, in terms of conductivity, are attributed to the greater surface area of the BVO@C, the electrocatalytic effect, and the semiconductor properties of the BVO, which, as a consequence, decrease the Rct, facilitating the transfer of electrons.
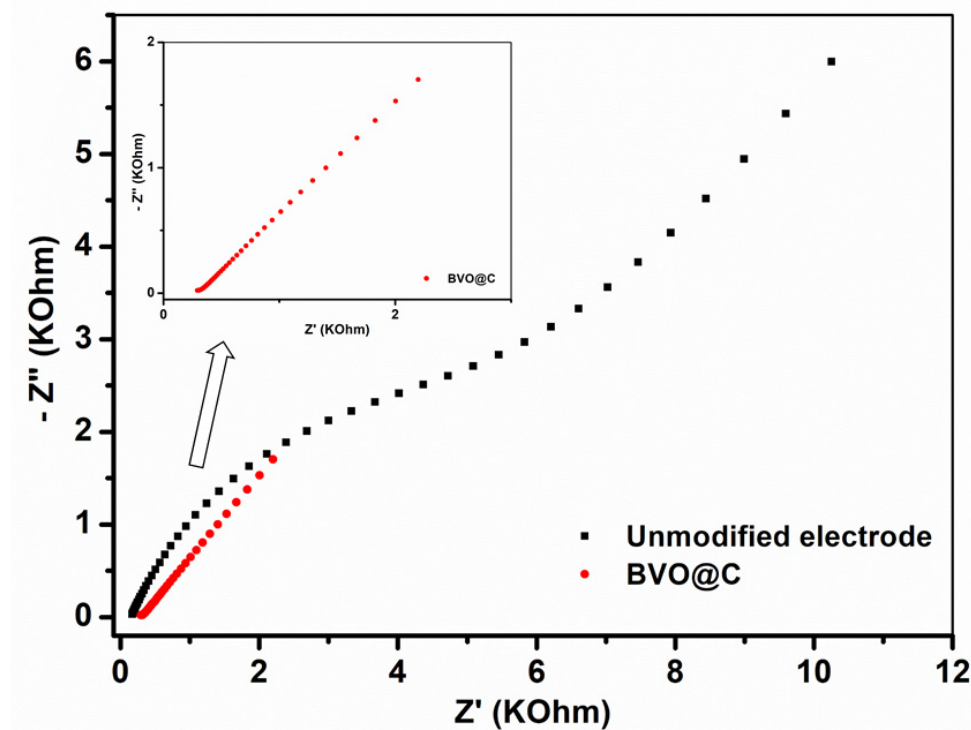

Figure 5. Nyquist diagram for the EIS measurements in 0.05 mol L^{-1} potassium ferrocyanide in 0.1 mol L^{-1} KCl for different electrode configurations.

Moreover, the diameter of the semicircle represents the difficulty of electron transfer in the solution and electrode system, providing information on the resistivity of the system and the electrochemical interphase.

In relation to Figure 5, the decrease in resistivity in the electrode BVO@C is much more significant than in the enlarged figure, and these results are interesting since, for the later use of the electrode, it is important that it has a low resistivity value, thus guaranteeing a higher rate of electronic transfer, a lower energy cost and, consequently, greater efficiency in the use of the electrode.

To observe the electrochemical response of the graphite and BVO@C electrodes, Cyclic Voltammetry (CV) analysis was performed in 0.05 mol L^{-1} potassium ferrocyanide in 0.1 mol L^{-1} KCl pH 7.0, and the result is illustrated in Figure 6.

The successive cyclic voltammograms scans for BVO@C and unmodified graphite are show in Figure 6. It can be observed the Ferro/Ferri E_{pa}/E_{pc} redox system is around 0.2 V, whereas the enlarged DE_p is related to low conductivity of pencil graphite. Moreover, the E_{pa} around 0.39 V refers to the oxidation of V^{4+} to V^{5+}, while in cathodic scanning the reduction of V^{5+} for V^{4+} was observed around 0.17 V, which associates with or is possibly due to the accumulation of charges in the conduction band, which was reported to have mixed V, Bi and O [43].

The hysteresis presented in the photocurrent profile can be linked to changes in pH within the structure of graphite. At more negative potentials, an increase exponential of the current is observed due to the release reaction of hydrogen by the reduction of water [44]. Since BVO is a semiconductor of the n-type, it is expected that it can be used in the oxidation reaction of water and oxygen production.
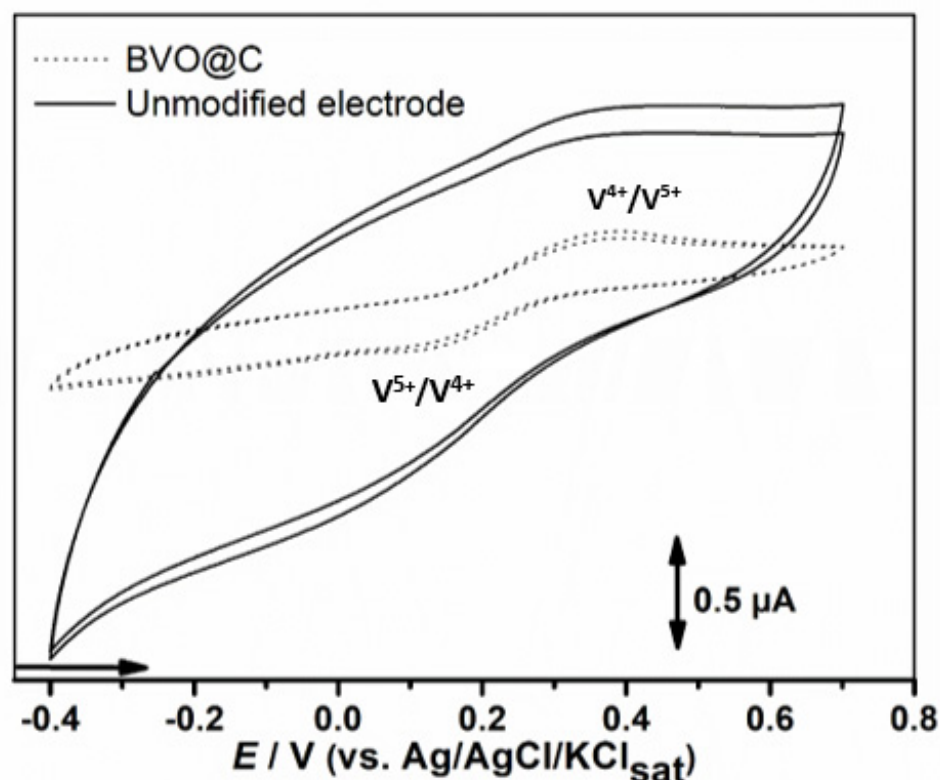
Figure 6. Cyclic voltammograms referring to two successive scans obtained for the different working electrode configurations. Reaction medium is 0.05 mol L^{-1} potassium ferrocyanide in 0.05 mol L^{-1} KCl.

Figure 6 shows that, after sanding the graphite and adding BVO, there was a possible decrease in the thickness of the graphite composite which leads to a smaller difference between the anodic and cathodic peak potentials (E_{pa} and E_{pc}, respectively); this, in addition to the increase in current values, probably indicates a lower electrical resistance of the BVO@C. It is noteworthy that the graphite composite layer directly influences the electron transfer resistance at the electrode/solution interface due to a lower conductivity of the graphite composite in relation to the BVO@C electrodes, the electrical conductivity of the latter being much higher. Similar results for a glassy carbon electrode modified with bismuth film were found [45].

In Table 2, the values of CPE (Constant Phase Element) suggest a non-ideal behavior of the capacitor, leading to the introduction of the phase element and Rp (bias resistance) that were obtained by VC and EIS methods, respectively, for the studied electrodes.

Table 2. Comparative EIS between unmodified electrodes and BVO@C electrode.

Electrodes	CPE	RP	Chi-Square (X^2)
Unmodified	1680 Ω	1.71 μF	0.047513
BVO@C	41.1 Ω	1.04 μF	0.0069898

The intersection of the semicircle at low frequencies with the Z′ (Ω) axis determined an Rp of 1680 Ω and an electrical double layer capacitance of 1.71 μF for the unmodified electrode, and an Rp of 41.1 Ω and an electrical double layer capacitance of 1.04 μF for the BVO@C. It is observed from the values found through Electrochemical Impedance Spectroscopy (EIS) that the resistivity values associated with resistance in parallel and the double layer decreased (about 97.5% reduction). These results can be related to the presence of BVO on the electrode surface since, in theory, the semiconductor would facilitate the

exchange of electrical charges, thus reducing the resistivity and consequently increasing the electronic exchange and the conductivity of the electrode.

In addition, a reduction in capacitance was observed of c.a. 40 times for the modified electrode, in comparison to the unmodified counterpart (Table 2). The decrease in the capacitive current is also easily noticeable in the CV comparison between electrodes (Figure 6). Because the CPE is intrinsically associated with the double-layer formed in the electrode's surface and the double-layer's capacitive current is a significant noise factor in electroanalysis, it is reasonable to assume that the modified electrode would yield better sensitivity and higher analytical signals.

Furthermore, the Chi-square values for the unmodified and modified electrodes were found to be 0.047513 and 0.0069898, respectively. Optimal values for Chi-square should be below (<0.001) for finding an equation or a model suitable for describing the electrical circuit equivalent, in order to minimize the sum of the squares. As we can see from the values obtained through the EIS, the value found for BVO@C (0.0069898) is closer to 0.001, that is, it presents a better quadratic correlation. Thus, we can infer that there was an improvement concerning the non-modified electrode since that showed values of 0.047513, well above the correlation values of interest.

Despite this, this parameter should not be the only criterion to be evaluated for a good fit. To have a better prediction of the circuit, it would be interesting to perform some diagnostic tests before performing the EIS. Among them, we can include linear polarization resistance trend, and low potential regime polarization trend for determining Rct and io, etc. In addition, the analysis of real and imaginary impedance variation with frequency change can also be used to predict interfacial processes. The variation of the adjusted phase angle (considering the resistance of the solution) with the frequency can be used to determine the existence of a diffusion control process.

3.4. Photoelectrocatalytic (PEC) and Elecrocatalytic (EC) Tests

To analyze the performance of BVO@C in relation to graphite without modification, electro-oxidation tests were performed. Experiments were carried out with standard graphite and with BVO@C, as can be seen in Figures 7A–C and 8. There was an increase in discoloration of RhB with the BVO@C modification compared with graphite without modification.

Figures 8 and 9 shows that the discoloration percentages for unmodified graphite, the BVO@C EC system, and the BVO@C PEC system at 5 min of treatment were 31.53%, 46.09% and 58.17%, respectively, reaching 95%, 98% and 99.64%, respectively, after 30 min of treatment. The results found in this work showed superior values of RhB degradation efficiency in relation to others presented in the literature [46–48].

This fact can be explained by the presence of BVO particles on the surface of the graphite, which favors electronic exchange on the active surface of the electrode while also significantly reducing the resistivity of the material. This can be explained by oxidation/reduction reactions that occur at the interface of the electrodes that make up the degradation system. These factors tend to increase the production of •OH radicals and other radicals in the reaction medium. There is also the synergistic factor [21] between the semiconductor and the chosen substrate, which makes this result even more efficient.
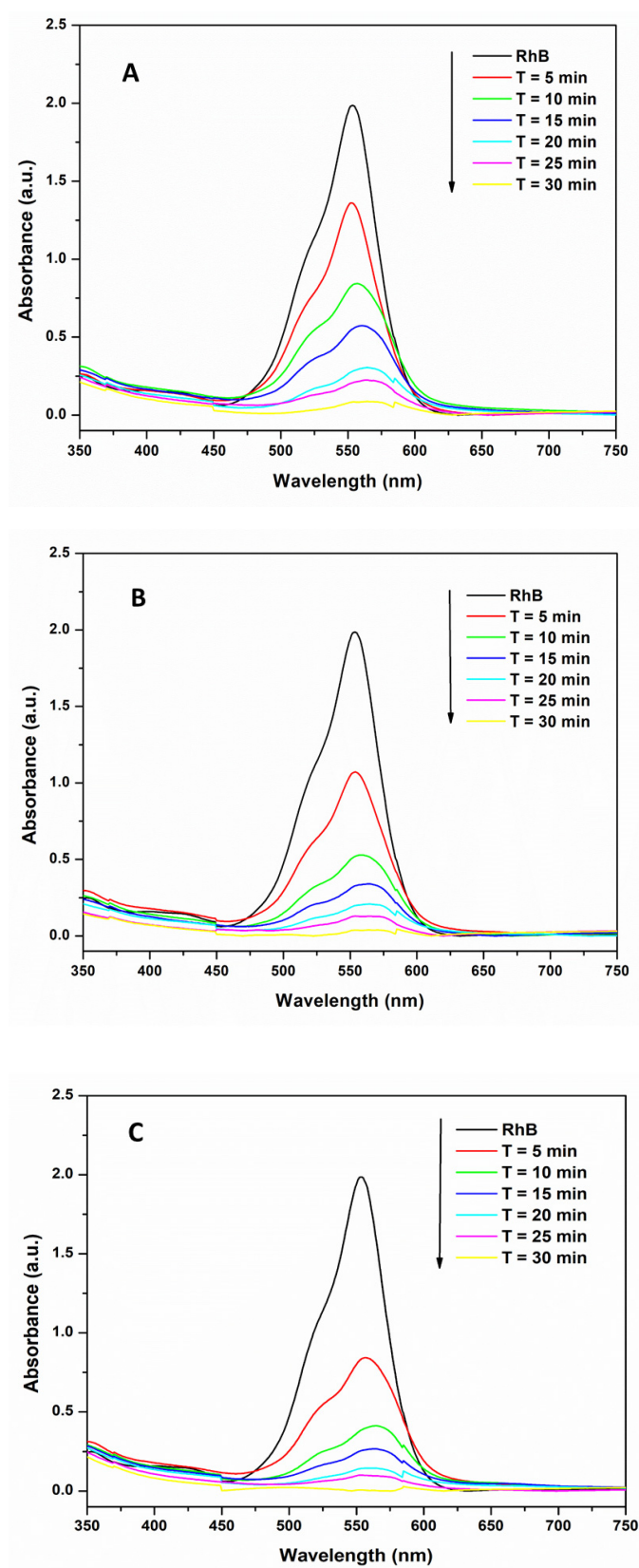
Figure 7. UV–Vis spectrum of RhB solution subjected to decolorization of RhB (20 mg L^{-1}) with unmodified graphite (**A**); BVO@C EC System (**B**); and BVO@C PEC System (**C**) at different reaction times using NaCl as electrolytic support (0.05 mol L^{-1}).
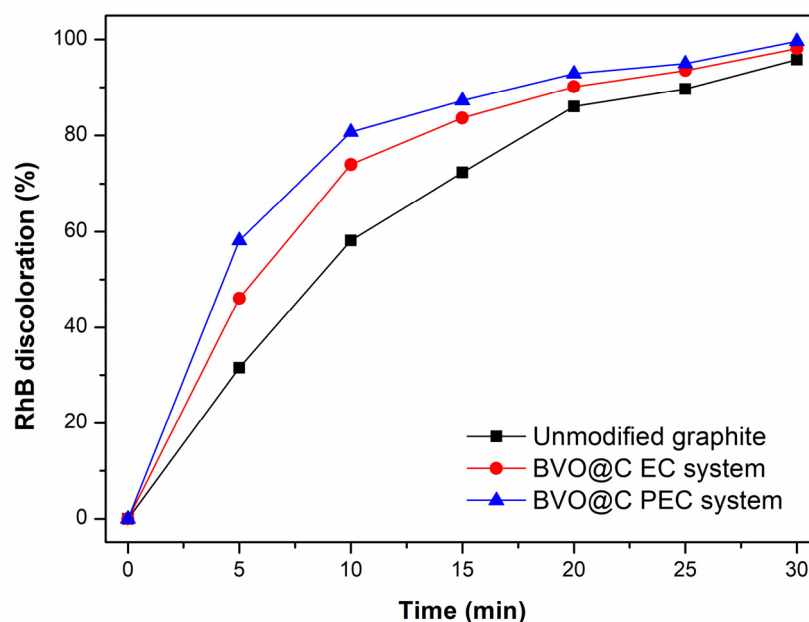
Figure 8. Electrocatalytic degradation of RhB solution (20 mg L^{-1}) in 30 min with unmodified graphite, BVO@C EC System and BVO@C PEC System, using NaCl as electrolytic support (0.05 mol L^{-1}), in pH of natural solution and at room temperature.
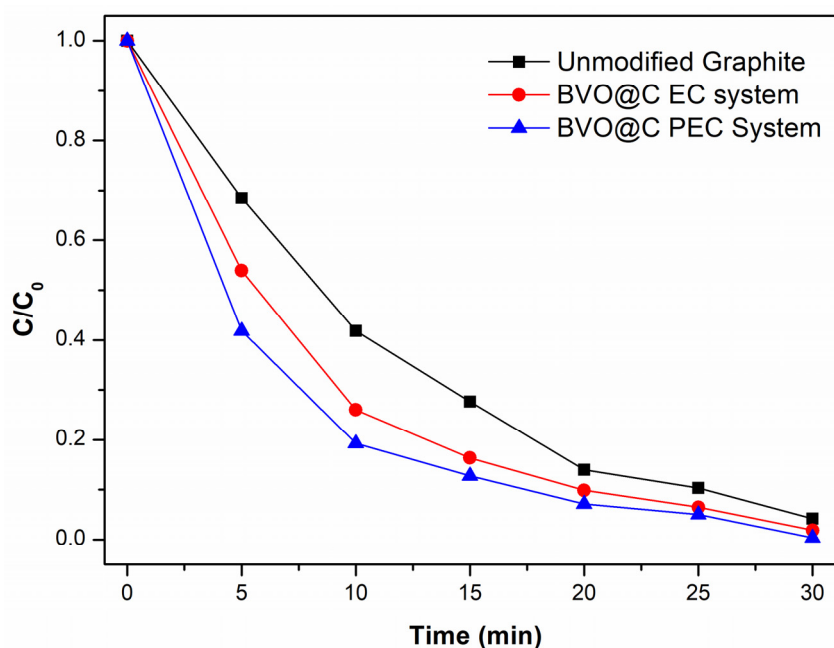

Figure 9. Degradation of pollutants during photoelectrocatalysis (PEC) and electrocatalysis (EC). Initial RhB concentration of 20 mg L^{-1}, using NaCl as electrolytic support (0.05 mol L^{-1}), pH of natural solution, at room temperature.

Based on the experimental results found, a possible reaction mechanism can be proposed for the degradation of RhB via PEC, and also the mechanism of interaction (hole scavenger) between graphite impregnated with BVO in relation to the hydroxyl radical (•OH) generation. Specifically, when the photoanode is under light irradiation (visible light, wavelength of approx. 520 nm), the electrons (e$^-$) present in the valence band (VB) of the BVO can be directed to the conduction band (CB), which leads to a greater number of holes (h$^+$) in VB from BVO. Subsequently, the electrons that were transferred to the CB from BVO can be quickly pulled into the CB from BVO@C under the anodic bias potential.

Then these electrons are transferred to the cathode through the external circuit in the PEC cell device, which decreases electron/hole pair recombination. Thus, the rapidly induced charge separation is managed in the interface between the BVO@C which can naturally strengthen the BVO photocatalytic performance when we have the BVO@C photoanode. Further studies are needed to identify with absolute clarity if there is a rational interaction mechanism between graphite and BVO in the generation of hydroxyl radical (●OH) through the oxidation of the water molecule via PEC. BVO@C can act in photoelectrocatalysis and water molecules can therefore be quickly oxidized in BVO@C to form free radicals, which are the oxidizing agents of RhB. Graphite/BVO's step division and cooperation is advantageous to accelerate the generation efficiency of hydroxyl radicals in the PEC system. In view of the results found, it is concluded that the attractive degradation presented in the PEC system could be attributed to the multiple synergistic effects of interaction between graphite and BVO particles. This synergism between the use of light and dye was also observed in other studies, which noted greater efficiency in the treatment of PEC systems compared to EC and PC systems [49–51]. Thus, further studies are suggested to identify possible intermediates and identify mechanisms of RhB degradation.

The results for the application of BVO@C in the PEC system showed higher values than the BVO@C EC system. Photoelectrocatalysis combines the advantages of photocatalytic oxidation (PC) and electrocatalytic oxidation (EC). When the potential difference was applied, along with visible light illumination, the photogenerated electrons due to band-ga were attracted to the cathode steering the system through the electrical circuit. In this way, the photogenerated holes were left free on the anode surface to oxidize organic materials. Thus, the recombination of the electron/hole pair was effectively avoided. Some studies [52,53] demonstrated that the sum of degradation rates for individual PC and EC systems were lower than for the PEC system at the same point, which indicates a synergistic effect in the PEC system. The results are important since the photoelectrochemical technique can be applied on a large-scale using sunlight as energy.

The kinetic study is an essential parameter in degradation studies. Therefore, this study was undertaken to predict the rate at which RhB is degraded from aqueous solution using the two different electrodes in the EC and PEC processes. According to previous studies [54–57], the discoloration dynamics of the RdB can be described by a model of pseudo-first-order kinetics. The graph of $\ln C_0/C$ (Figure 10) as a function is shown in a straight line. Studying the slope of this line in linear regression corresponds to the apparent first-order rate constant (K).

In EC reactions with unmodified graphite and with BVO@C, lower values of k (0.10272 and 0.12221 min^{-1}, respectively) were observed relative to the application of BVO@C in the PEC system (k = 0.15022 min^{-1}). This can be explained by the oxidation/reduction reactions that appear at the interface of the electrodes that compose the degradation system, as a greater electronic exchange favored by the presence of the semiconductor BVO on the surface of the substrate may be associated with the higher values of k found for BVO@C.
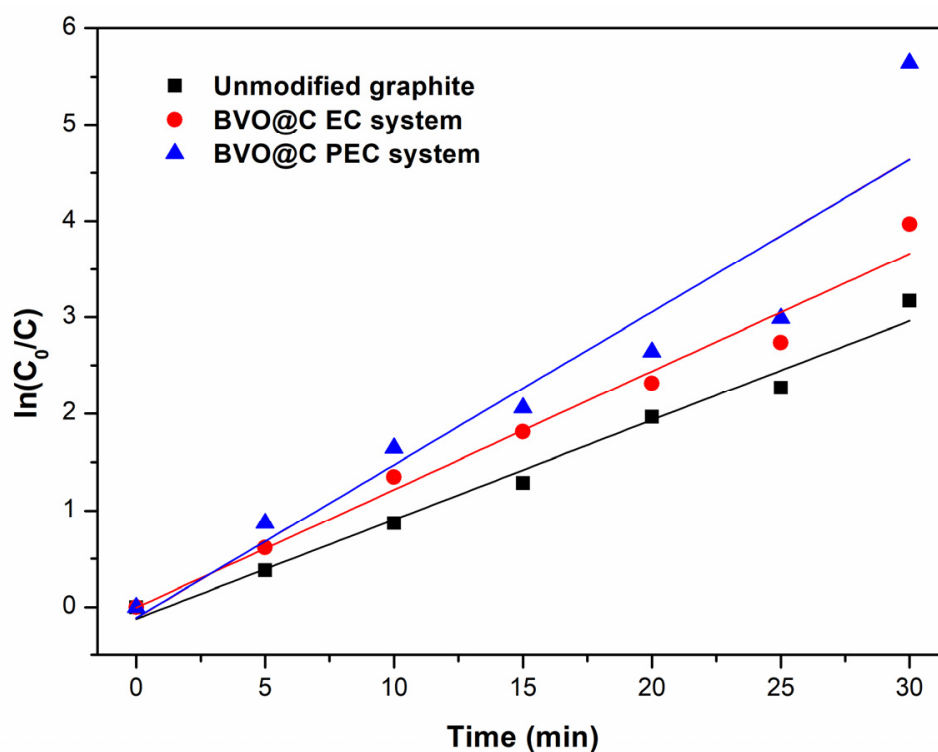
Figure 10. Kinetic plots of apparent first-order linear transform ln (C_0/C) against time of irradiation (t) with unmodified graphite and BVO@C.

The kinetics of the reactions is influenced by various parameters such as catalyst mass, oxygen pressure, and temperature pollutant concentration, which were not discussed because they are not described within the scope of the present work and can be evaluated in later work [55].

3.5. Reuse Cycles

The reuse of the electrode in subsequent experiments is one of the main advantages of using this type of material [58]. The reuse of the electrode is important in industrial-scale operations, such as wastewater treatment. This characteristic configures a high application versatility and high treatment efficiency, thus reducing the operational costs related to the electrode. In addition, the reuse of electrodes meets the principles of green chemistry, considering the environment; this is increasingly important, as such recycling tends to minimize waste generation and save materials considered high-added value as BDD electrodes. The evaluation in relation to the reuse cycles of the BVO@C electrode was performed as a function of the degradation rate of RhB (expressed as a percentage) over 30 min (Figure 11).

The electrode presented a high rate of degradation of RhB, with about 90% degradation of the dye maintained up to the 4th reuse cycle. After the 5th cycle, there was a slight decrease in the efficiency of the electrode, reaching approximately 80% RhB degradation after the 9th cycle of use. One explanation for this phenomenon is to consider that organic molecules or reactive intermediates are adsorbed on the surface of the particle electrodes and the wear of the particles on the electrodes can be caused in the process of use. The reuse rates of working electrodes in PEC degradation change according to the material used as the catalyst and the type of target compound; nonetheless, these have excellent rates of organic compost degradation or inactivation of bacteria after several cycles of degradation [59,60].
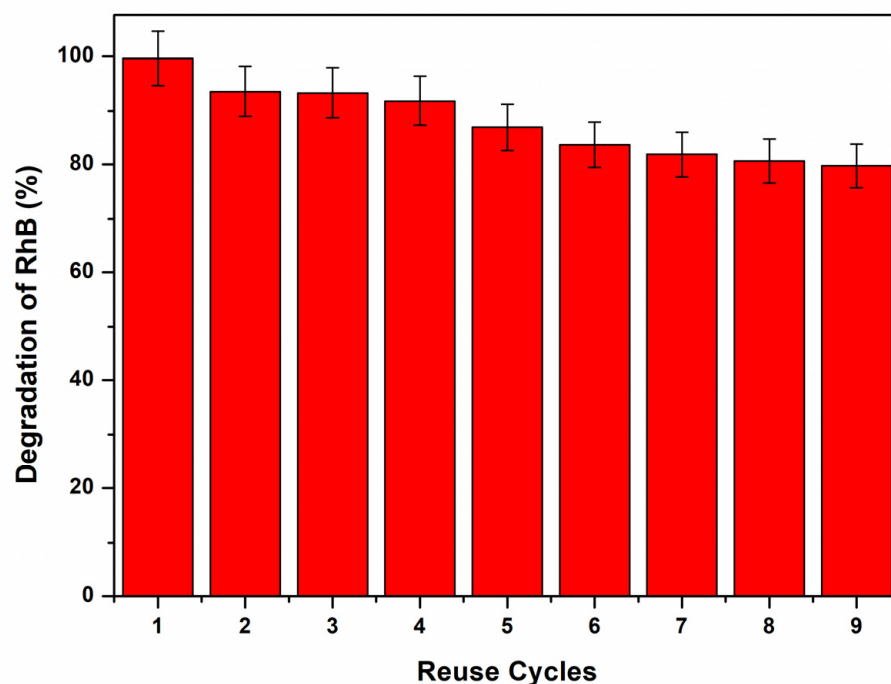
Figure 11. Effect of reuse cycles of the BVO@C electrode in the PEC system on the removal of RhB in 30 min.

4. Conclusions

A new electrode consisting of pencil graphite deposited with bismuth vanadate (BVO@C) particles was successfully synthesized by the deposition method. The results of the characterization step demonstrated the presence of BVO groups on the surface of pencil lead. In addition, it was possible to optimize the synthesis of the graphite electrode with BVO by varying the concentration of BVO and the contact time of the graphite with the BVO/water solution. When evaluating the response surface, we noticed two trends that seemed to be antagonistic towards maximizing the efficiency of RhB degradation; one with a shorter contact time of graphite with the solution and a higher concentration of BVO, and the other with a longer contact time of graphite with the solution and lower values of BVO concentration. As the contact time is considered high (24, 48, 72 h), our preference was to work with higher concentration values and a shorter contact time with the solution.

The results obtained by SEM/EDS showed specific peaks referring to Bi, V and O, thus confirming the presence of BVO particles on the graphite electrode surface. Furthermore, different sizes of BVO particles were found on the surface, demonstrating that the distribution was not homogeneous; in addition, there was not a complete coating of the graphite, with the formation of a thin homogeneous layer on the graphite surface. These results may be related to the PDI value found for the water/BVO solution (0.456) indicating that the solution is not prone to the formation of agglomerates, which may be intrinsically linked to the difficulty of forming a homogeneous deposition on the surface of the electrode. The zeta potential found in the BVO@C material was found to be $\zeta = -22.2$ mV, indicating that the surface charge of the particles used to modify the graphite presented negative charges. This parameter is important, since, theoretically, electrodes with negative charges would present a greater degradation efficiency in relation to cationic compounds, as is the case of RhB.

The unmodified electrode and BVO@C were electrochemically characterized through EIS and CV, confirming that the electrodes modified with BVO nanoparticles presented better electrochemical performance than the electrodes without modification. The BVO@C showed greater electroactive surface area, and lower electron transfer resistance, considerably increasing the electron transfer rate with a higher current gain relative to the

unmodified electrode due to the higher conductivity of BVO, ensuring more excellent stability of the modifier layer on the electrode surface.

Degradation tests (EC and PEC) using the unmodified electrode and BVO@C confirmed that the synthesized modified electrode degraded the target compound (RhB) more efficiently than the unmodified electrode. The application of BVO@C in the PEC process showed better results than when the same electrode was applied in the EC process. The degradation percentages for unmodified graphite and BVO@C applied to EC and PEC at 5 min of treatment were 31.53%, 46.09%, and 58.17%, and reached 95%, 98%, and 99.64%, respectively, at 30 min of treatment. First-order apparent velocity constant values were determined (0.10272, 0.12221, and 0.15022 m^{-1}, respectively). The values found may be related to the presence of BVO on the electrode surface which, in theory, would facilitate electronic exchange and the production of radicals (●OH), thus increasing the degradation of the organic pollutant. In addition, the electrode showed good stability, with 9 reuse cycles and maintaining the degradation efficiency above 80%. This result is important because the more stable the electrode, the lower the cost of manufacturing new electrodes.

The development of a new modified electrode prepared with 2 mm pencil graphite modified with BVO nanoparticles by the contact deposition method is considered an easy, fast, low-cost and simple method. Experiments aimed at testing its potential use in several electrochemical applications of clinical, pharmaceutical and environmental interest were successfully performed. In summary, these results indicate the excellent performance of BVO@C for water remediation applications in the degradation of persistent contaminants such as RhB. Furthermore, the ease of synthesis opens the door to future applications to cost-effectively degrade a wide range of emerging contaminants as well as other possible applications.

Author Contributions: Conceptualization, B.G.I., E.d.S.G., F.C. and G.F.T.; methodology, G.F.T., A.S.G., A.R.d.S. and B.G.I.; software, I.Y.L.d.M. and L.M.D.; formal analysis, G.F.T., L.M.D. and A.G.C.C.; investigation, B.G.I.; resources, E.d.S.G.; writing—preparation of the original draft, B.G.I.; writing—review and editing, G.F.T., E.d.S.G., V.S.S. and S.B.d.O.; supervision, E.d.S.G.; project management, E.d.S.G.; funding acquisition, E.d.S.G. All authors have read and agreed to the published version of the manuscript.

Institutional Review Board Statement: Not applicable.

Informed Consent Statement: Not applicable.

Data Availability Statement: Not applicable.

Conflicts of Interest: The authors declare no conflict of interest.

References

1. Wang, T.; Li, C.; Xie, X.; Lu, B.; He, Z.; Liang, S.; Zhou, J. Anode Materials for Aqueous Zinc Ion Batteries: Mechanisms, Properties, and Perspectives. *ACS Nano* **2020**, *14*, 16321–16347. [CrossRef] [PubMed]
2. Li, C.; Zhang, B.; Liu, Q. N-eicosane/expanded graphite as composite phase change materials for electro-driven thermal energy storage. *J. Energy Storage* **2020**, *29*, 101339. [CrossRef]
3. Lv, Y.; Han, C.; Zhu, Y.; Zhang, T.; Yao, S.; He, Z.X.; Dai, L.; Wang, L. Nanostructured N-doped carbon materials for vanadium redox flow battery: Properties, structures, and perspectives. *J. Mater. Sci. Technol.* **2021**, *75*, 96–109. [CrossRef]
4. Cuerda-Correa, E.M.; Alexandre-Franco, M.F.; Fernández-González, C. Advanced Oxidation Processes for the Removal of Antibiotics from Water: An Overview. *Water* **2020**, *12*, 102. [CrossRef]

5. Ruifeng, R.; Pengfei, T.; Lu, Y.; Huanhuan, Z.; Mingyuan, Z.; Jiaoyang, C.; Hele, L.; Jun, P. Controlled fabrication of bismuth vanadate nanotubes for visible light photocatalysis. *Mater. Lett.* **2022**, *324*, 132742.

6. Akhter, P.; Arshad, A.; Saleem, A.; Hussain, M. Recent Development in Non-Metal-Doped Titanium Dioxide Photocatalysts for Different Dyes Degradation and the Study of Their Strategic Factors: A Review. *Catalysts* **2022**, *12*, 1331. [CrossRef]

7. Agrawal, A.; Siddiqui, S.A.; Soni, A.; Sharma, G.D. Advancements, frontiers and analysis of metal oxide semiconductor, dye, electrolyte and counter electrode of dye sensitized solar cell. *Sol. Energy* **2022**, *233*, 378–407. [CrossRef]

8. Arora, I.; Chawla, H.; Chandra, A.; Sagadevan, S.; Garg, S. Advances in the strategies for enhancing the photocatalytic activity of TiO$_2$: Conversion from UV-light active to visible-light active photocatalyst. *Inorg. Chem. Commun.* **2022**, *143*, 109700. [CrossRef]

9. Vaya, D.; Kaushik, B.; Surolia, P.K. Recent advances in graphitic carbon nitride semiconductor: Structure, synthesis and applications. *Mater. Sci. Semicond. Process.* **2021**, *137*, 106181. [CrossRef]

10. Moharam, M.M.; El Shazly, A.N.; Anand, K.V.; Rayan, D.E.-R.A.; Mohammed, M.K.A.; Rashad, M.M.; Shalan, A.E. Semiconductors as Effective Electrodes for Dye Sensitized Solar Cell Applications. *Top. Curr. Chem.* **2021**, *379*, 20. [CrossRef]

11. Nayak, S.; Parida, K. Recent Progress in LDH@Graphene and Analogous Heterostructures for Highly Active and Stable Photocatalytic and Photoelectrochemical Water Splitting. *Chem. Asian J.* **2021**, *16*, 2211–2248. [CrossRef]

12. Jana, S.; Konar, S.; Mitra, B.C.; Mondal, A.; Mukhopadhyay, S. Fabrication of a new heterostructure Au/Pt/SnO$_2$: An excellent catalyst for fast reduction of para-nitrophenol and visible light assisted photodegradation of dyes. *Mater. Res. Bull.* **2021**, *141*, 111351. [CrossRef]

13. Norizan, M.N.; Abdullah, N.; Halim, N.A.; Demon SZ, N.; Mohamad, I.S. Heterojunctions of rGO/Metal Oxide Nanocomposites as Promising Gas-Sensing Materials—A Review. *Nanomaterials* **2022**, *12*, 2278. [CrossRef]

14. Kouvelis, K.; Kampioti, A.A.; Petala, A.; Frontistis, Z. Degradation of Sulfamethoxazole Using a Hybrid CuOx–BiVO$_4$/SPS/Solar System. *Catalysts* **2022**, *12*, 882. [CrossRef]

15. Sun, H.; Zou, C.; Tang, W. Designing double Z-scheme heterojunction of g-C$_3$N$_4$/Bi$_2$MoO$_6$/Bi$_2$WO$_6$ for efficient visible-light photocatalysis of organic pollutants. *Colloids Surf. A Physicochem. Eng. Asp.* **2022**, *654*, 130105. [CrossRef]

16. Wang, Y.; Tang, Y.; Sun, J.; Wu, X.; Liang, H.; Qu, Y.; Jing, L. BiFeO$_3$/Bi$_2$Fe$_4$O$_9$ S-scheme heterojunction hollow nanospheres for high-efficiency photocatalytic o-chlorophenol degradation. *Appl. Catal.* **2022**, *319*, 121893. [CrossRef]

17. Luo, Y.; Wang, K.; Hu, T.; Liu, X. Controlled synthesis of palygorskite/Bi$_5$O$_7$I hybrid microspheres with high efficient photodegradation of antibiotics. *Colloids Surf. A Physicochem. Eng. Asp.* **2021**, *616*, 126225. [CrossRef]

18. Wu, L.; Yue, X.; Chang, Y.; Wang, K.; Zhang, J.; Sun, J.; Wei, Z.; Kowalska, E. Photocatalytic Degradation of Tetracycline under Visible Light Irradiation on BiVO$_4$ Microballs Modified with Noble Metals. *Catalysts* **2022**, *12*, 1293. [CrossRef]

19. Fan, H.; Yi, G.; Zhang, Z.; Zhang, X.; Li, P.; Zhang, C.; Chen, L.; Zhang, Y.; Sun, Q. Fabrication of Ag particles deposited BiVO$_4$ photoanode for significantly efficient visible-light driven photoelectrocatalytic degradation of β-naphthol. *J. Environ. Chem. Eng.* **2022**, *10*, 107221. [CrossRef]

20. Lotfi, S.; Ouardi, M.E.; Ahsaine, H.A.; Assani, A. Recent progress on the synthesis, morphology and photocatalytic dye degradation of BiVO$_4$ photocatalysts: A review. *Catal. Rev.* **2022**, 1–45.

21. Zhang, M.; Shao, C.; Li, X.; Zhang, P.; Sun, Y.; Su, C.; Zhang, X.; Ren, J.; Liu, Y. Carbon-modified BiVO$_4$ microtubes embedded with Ag nanoparticles have high photocatalytic activity under visible light. *Nanoscale* **2012**, *4*, 7501–7508. [CrossRef] [PubMed]

22. Ghazkoob, N.; Shoushtari, M.Z.; Kazeminezhad, I.; Baghal, S.L. Investigation of structural, magnetic, optical and photocatalytic properties of zinc ferrite nanowires/bismuth vanadate composite. *J. Alloys Compd.* **2022**, *900*, 163467. [CrossRef]

23. Radoor, S.; Karayil, J.; Jayakumar, A.; Nandi, D.; Parameswaranpillai, J.; Lee, J.; Shivanna, J.M.; Nithya, R.; Siengchin, S. Adsorption of Cationic Dye onto ZSM-5 Zeolite-Based Bio Membrane: Characterizations, Kinetics and Adsorption Isotherm. *J. Polym. Environ.* **2022**, *30*, 3279–3292. [CrossRef]

24. Ismail, M.; Khan, M.; Khan, S.B.; Akhtar, K.; Asiri, A.M. Catalytic reduction of picric acid, nitrophenols and organic azo dyes via green synthesized plant supported Ag nanoparticles. *J. Mol. Liq.* **2018**, *268*, 87–101. [CrossRef]

25. Kadam, A.N.; Babu, B.; Lee, S.W.; Kim, J.; Yoo, K. Morphological guided sphere to dendrite BiVO$_4$ for highly efficient organic pollutant removal and photoelectrochemical performance under solar light. *Chemosphere* **2022**, *305*, 135461. [CrossRef]

26. Gomes, L.E.; Plaça, L.F.; Rosa, W.S.; Gonçalves, R.V.; Ullah, S.; Wender, H. Increasing the Photocatalytic Activity of BiVO$_4$ by Naked Co(OH)$_2$ Nanoparticle Cocatalysts. *Photochem* **2022**, *2*, 866–879. [CrossRef]

27. Shen, X.; Zhao, L.; Fan, W.; Ren, J.; Wang, Q.; Wang, A.; Shang, D.; Zhu, W. Efficient photoelectrochemical water oxidation of cobalt phthalocyanine decorated BiVO$_4$ photoanode by improving kinetics. *Appl. Surf. Sci.* **2021**, *564*, 150463. [CrossRef]

28. Fard, S.G.; Haghighi, M.; Shabani, M. Facile one-pot ultrasound-assisted solvothermal fabrication of ball-flowerlike nanostructured (BiOBr)$_x$(Bi7O9I3)$_{1−x}$ solid-solution for high active photodegradation of antibiotic levofloxacin under sun-light. *Appl. Catal. B Environ.* **2019**, *248*, 320–331. [CrossRef]

29. Aguilera-Ruiz, E.; Zambrano-Robledo, P.; Vazquez-Arenas, J.; Cruz-Ortiz, B.; Peral, J.; García-Pérez, U.M. Photoactivity of nanostructured spheres of BiVO$_4$ synthesized by ultrasonic spray pyrolysis at low temperature. *Mater. Res. Bull.* **2021**, *143*, 111447. [CrossRef]

30. Rendevski, S.J.; Dyussenbekov, A.M.; Nurlanov, F.N. A practical lab on composite materials and sensors, enhanced with electrical percolation threshold theory. *Eur. J. Phys.* **2020**, *41*, 055802. [CrossRef]

31. Hartmann, L.A. Strategic minerals from southern Brazil: Geology of amethyst and agate geodes. In *Technology for the Gem, Jewelry and Mining Sector*; Hartmann, L.A., da Silva, J.T., Eds.; Federal University of Rio Grande do Sul, Institute of Geosciences: Porto Alegre, Brazil, 2010; pp. 30–39.

32. Internacional Centre for Difraction Data. Available online: https://www.icdd.com/pdfsearch/ (accessed on 22 September 2021).

33. Malashchonak, M.V.; Streltsov, E.A.; Kuliomin, D.A.; Kulak, A.I.; Mazanik, A.V. Monoclinic bismuth vanadate band gap determination by photoelectrochemical spectroscopy. *Mater. Chem. Phys.* **2017**, *201*, 189–193. [CrossRef]

34. Wei, T.; Jin, Z.; Li, F.; Sun, Z.; Xu, L. Solar water oxidation using TaON–BiVO$_4$ photoanodes functionalized with WO$_3$. *J. Chem. Soc.* **2021**, *50*, 1780–1787. [CrossRef]

35. Neto, J.S.O.; Lima, A.F.; Limeira, Y.F.X.; Cruz, C.P.T. Characterization of historical mortar sin the 18th century house landmark: A case study. *Braz. J. Dev.* **2021**, *7*, 28270–28286. [CrossRef]

36. Park, H.; Kim, M.; Bae, T.; Yuan, J.; Yu, J. Fabrication of binder-free pencil trace electrode for lithium-ion battery: Simplicity and high performance. *Langmuir* **2016**, *18*, 4415–4423. [CrossRef]

37. Rani, P.; Kumar, K.S.; Pathak, A.D.; Sharma, C.S. Pyrolyzed pencil graphite coated cellulose paper as an interlayer: An effective approach for high-performance lithium-sulfur battery. *Appl. Surf. Sci.* **2020**, *533*, 147483. [CrossRef]

38. El-Katori, E.E.; Kasim, E.A.; Ali, D.A. Sol–gel synthesis of mesoporous NiO/ZnO heterostructure nanocomposite for photocatalytic and anticorrosive applications in aqueous media. *Colloids Surf. A Physicochem. Eng. Asp.* **2021**, *636*, 128153. [CrossRef]

39. Jana, A.K. Solar cells based on dyes. *J. Photochem. Photobiol. A Chem.* **2000**, *132*, 1–17. [CrossRef]

40. Soltani, T.; Lee, B.K. Ag-doped BiVO$_4$/BiFeO$_3$ photoanode for highly efficient and stable photocatalytic and photoelectrochemical water splitting. *Sci. Total Environ.* **2020**, *736*, 138640. [CrossRef]

41. Liu, T.; Zhang, X.; Guan, J.; Catlow CR, A.; Walsh, A.; Sokol, A.A.; Buckeridge, J. Insight into the Fergusonite–Scheelite Phase Transition of ABO$_4$-Type Oxides by Density Functional Theory: A Case Study of the Subtleties of the Ground State of BiVO$_4$. *Chem. Mater.* **2022**, *34*, 5334–5343. [CrossRef]

42. Hebert, J.; Wang, L.; Wang, X.; Baker, J.; Rivera, N.; Troedel, M.; Li, Z. Mechanisms of safranin O interaction with 1:1 layered clay minerals. *Sep. Sci. Technol.* **2020**, *56*, 1985–1995. [CrossRef]

43. Mascaro, L.H.; Pockett, A.; Mitchels, J.M.; Peter, L.M.; Cameron, P.J.; Celorrio, V.; Fermin, D.J.; Sagu, J.S.; Wijayantha, K.G.U.; Kociok-Kohn, G.; et al. One-step preparation of the BiVO$_4$ film photoelectrode. *J. Solid State Electrochem.* **2014**, *19*, 31–35. [CrossRef]

44. Rullens, F.; Laschewsky, A.; Devillers, M. Bulk and Thin Films of Bismuth Vanadates Prepared from Hybrid Materials Made from an Organic Polymer and Inorganic Salts. *Chem. Mater.* **2006**, *18*, 771–777. [CrossRef]

45. Rafatullah, M.; Sulaiman, O.; Hashim, R.; Ahmad, A. Adsorption of methylene blue on low-cost adsorbents: A review. *J. Hazard. Mater.* **2010**, *177*, 70–80. [CrossRef] [PubMed]

46. Du, L.; Wu, J.; Hu, C. Electrochemical oxidation of rhodamine B on RuO$_2$–PdO–TiO$_2$/Ti electrode. *Electrochim. Acta.* **2012**, *68*, 69–73. [CrossRef]

47. Baddouh, A.; Bessegato, G.G.; Rguiti, M.M.; El Ibrahimi, B.; Bazzi, L.; Hilali, M.; Zanoni, M.V.B. Electrochemical decolorization of Rhodamine B dye: Influence of anode material, chloride concentration and current density. *J. Environ. Chem. Eng.* **2018**, *6*, 2041–2047. [CrossRef]

48. Honeychurch, K.C. Voltammetric Behaviour of Rhodamine B at a Screen-Printed Carbon Electrode and Its Trace Determination in Environmental Water Samples. *Sensors* **2022**, *22*, 4631. [CrossRef]

49. Lee, J.; Liu, X.; Kumar, A.; Hwang, Y.; Lee, E.; Yu, J.; Kim, Y.D.; Lee, H. Phase-selective active sites on ordered/disordered titanium dioxide enable exceptional photocatalytic ammonia synthesis. *Chem. Sci.* **2021**, *12*, 9619–9629. [CrossRef]

50. Lyu, J.; Liu, X.; Chen, Y.; Li, H.; Li, R.; Dong, X.; Lee, H.; Ma, H. Highly Enhanced Photoelectrocatalytic Oxidation via Cooperative Effect of Neighboring Two Different Metal Oxides for Water Purification. *J. Phys. Chem. C* **2020**, *124*, 11525–11535. [CrossRef]

51. Sathishkumar, K.; Kannan, V.R.; Alsalhi, M.S.; Rajasekar, A.; Devanesan, S.; Narenkumar, J.; Kim, W.; Liu, X. Intimately coupled gC3N4 photocatalysis and mixed culture biofilm enhanced detoxification of sulfamethoxazole: Elucidating degradation mechanism and toxicity assessment. *Environ. Res.* **2022**, *214*, 113824. [CrossRef]

52. Zhou, B.; Qu, J.; Zhao, X.; Liu, H. Fabrication and photoelectrocatalytic properties of nanocrystalline monoclinic BiVO$_4$ thin-film electrode. *J. Environ. Sci.* **2011**, *23*, 151–159. [CrossRef]

53. Pelegrini, R.; Peralta-Zamora, P.; de Andrade, A.R.; Reyes, J.; Durán, N. Electrochemically assisted photocatalytic degradation of reactive dyes. *Appl. Catal.* **1999**, *22*, 83–90. [CrossRef]

54. Wang, N.; Hu, Q.; Du, X.; Xu, H.; Hao, L. Study on decolorization of Rhodamine B by raw coal fly ash catalyzed Fenton-like process under microwave irradiation. *Adv. Powder Technol.* **2019**, *30*, 2369–2378. [CrossRef]

55. Zhu, X.; Zhang, L.; Zou, G.; Chen, Q.; Guo, Y.; Liang, S.; Hu, L.; North, M.; Xie, H. Carboxylcellulose hydrogel confined-Fe$_3$O$_4$ nanoparticles catalyst for Fenton-like degradation of Rhodamine B. *Int. J. Biol. Macromol.* **2021**, *180*, 792–803. [CrossRef]

56. Nguyen, L.H.; Van, H.T.; Ngo, Q.N.; Thai, V.N.; Hoang, V.H.; Hai, N.T.T. Improving Fenton-like oxidation of Rhodamin B using a new catalyst based on magnetic/iron-containing waste slag composite. *Environ. Technol. Innov.* **2021**, *23*, 101582. [CrossRef]

57. Sun, X.-F.; Wang, S.-G.; Liu, X.-W.; Gong, W.-X.; Bao, N.; Gao, B.-Y.; Zhang, H.-Y. Biosorption of Malachite Green from aqueous solutions onto aerobic granules: Kinetic and equilibrium studies. *Bioresour. Technol.* **2008**, *99*, 3475–3483. [CrossRef]

58. Geraldino, H.C.; Freitas, T.K.; Manholer, D.D.; França, F.; Oliveira, J.H.; Volnistem, E.A.; Garcia, J.C. Electrochemical generation of H_2O_2 using gas diffusion electrode improved with rGO intensified with the Fe_3O_4/GO catalyst for degradation of textile wastewater. *J. Water Process. Eng.* **2020**, *36*, 101377. [CrossRef]

59. Kumar, P.S.; Selvakumar, M.; Babu, S.G.; Induja, S.; Karuthapandian, S. CuO/ZnO nanorods: An affordable efficient p-n heterojunction and morphology dependent photocatalytic activity against organic contaminants. *J. Alloys Compd.* **2017**, *701*, 562–573. [CrossRef]

60. Rao, M.P.; Wu, J.J.; Asiri, A.M.; Anandan, S.; Ashokkumar, M. Photocatalytic properties of hierarchical CuO nanosheets synthesized by a solution phase method. *J. Environ. Sci.* **2018**, *69*, 115–124. [CrossRef]